Supporting Information

to

Steric Influence of Salicylaldehyde-based Schiff Base Ligands in the Formation of *trans*-$[Re(PR_3)_2(\text{Schiff Base})]^+$ Complexes

Jakob E. Baumeister, Andrew W. Mitchell, Steven P. Kelley, Charles L. Barnes, Silvia S. Jurisson*

Department of Chemistry, University of Missouri, Columbia, MO 65211

Section 1. SCXRD refinement details for compounds **2**, **3**•CH_3OH, **5**, **7**•2.333CH_3OH, and **8-11 (Table S1**); ORTEP representations for compounds **2**, **5**, **8**, **9**, **10** (**Figures S1-S5**)

Section 2. ^{1}H-NMR spectra for compounds **2-11** (**Figures S6-S21**)

Section 3. Cyclic voltammograms for compounds **2-7** (**Figures S22-S28**)

Supplemental Information Section 1. *SCXRD refinement details for compounds* ***2****,* ***3•****CH_3OH,* ***5****, 7•2.333CH_3OH, and* ***8-11***

Compounds **2**, **3•**CH_3OH, **5**, and **11** were solved by iterative dual space recycling as implemented in SHELXT v. 2014/5.[1] Compounds **7•**2.333CH_3OH, **8**, **9**, and **10** were solved by direct methods as implemented in SHELXS.[2] All structures were refined by full-matrix least squares refinement against F^2 using SHELXL v. 2017/1.[3] Full occupancy non-hydrogen atoms were refined anisotropically to convergence. Hydrogen atoms were placed in calculated positions and constrained to ride on the carrier atoms; a riding-rotating model was used for methyl group hydrogen atoms. $[PF_6]^-$ ions in **2** and **5** and two ethyl groups from a $P(Et)_3$ ligand in **5** were found to be disordered over two positions; the relative occupancies were constrained to add to 1 and refined to values of 87.5%, 69.3%, 53.2%, and 54.3% for the major parts of all four groups, respectively. A total of five distance restraints were used to keep the disordered groups in **5** near reasonable values. Due to systematic errors in the intensities for **11** caused by satellite crystals, rigid group restraints were used to keep the anisotropic thermal ellipsoids for the terminal Re≡O oxygen atom within reasonable values.[4] For compounds **3•**CH_3OH and **7•**2.333CH_3OH, contributions to scattering from highly disordered solvent molecules were determined and removed using PLATON SQUEEZE.[5] The structure of **3•**CH_3OH was found to contain 70 electrons per unit cell distributed across 256 $Å^3$ of void space, in good agreement with the expected values for four methanol molecules (72 electrons). For **7•**2.333CH_3OH, 336 electrons were found distributed through a total void volume of 1902 $Å^3$, equivalent to 18.667 methanol molecules per unit cell (7 methanol molecules per 3 molecules of the metal complex).

For Compound **2**, the thermal ellipsoid of the Cl^- ion is significantly greater than the average values for other non-hydrogen atoms in the structure; greater thermal motion is chemically reasonable for this moiety as it is situated within the disordered solvent void. Compounds **8** and **11** contain significant difference map peaks in chemically unreasonable positions, which are likely caused by extra intensity from diffraction by unremovable satellite crystals. This is supported by the fact that $|F_{obs}| > |F_{calc}|$ for the most disagreeable reflections. For compound **11**, which crystallized in the form of highly intergrown clumps, this problem is especially severe; nearly complete powder diffraction rings are observed on almost every frame of the data. Nevertheless, the data that was able to be obtained for **11** could be reliably indexed to a single unit cell and refined anisotropically as a structure fully consistent with the NMR data. Since both morphological inspection and the appearance of the diffraction data suggested the crystal of **11** is likely a single crystal core heavily coated in smaller, randomly oriented satellites, improving the model with de-twinning was not feasible.

References

1. Sheldrick, G. M., *Acta Crystallogr. A* **2015,** *71*, 3-8.
2. Sheldrick, G. M. *SHELXS, v.2013-1*, 2013.
3. Sheldrick, G. M., *Acta Crystallogr. C* **2015,** *71*, 3-8.
4. Thorn, A.; Dittrich, B.; Sheldrick, G. M., *Acta Crystallogr. A* **2012,** *68*, 448-451.
5. Spek, A. L., *Acta Crystallogr. C* **2015,** *71*, 9-18.

Table S1. *X-ray crystal data, data collection parameters, and refinement parameters for* ***2***, ***3***•CH_3OH, ***5***, ***7***•2.333CH_3OH, *and* ***8-11***.

	2	**3**•CH_3OH	**5**	**7**•2.333CH_3OH	**8**	**9**	**10**	**11**
CCDC	1910610	1910611	1910612	1910613	1910614	1910615	1910616	1912253
formula	$C_{28}H_{44}F_6N_2O_2P_3Re$	$C_{44}H_{44}ClN_2O_2P_2Re$	$C_{30}H_{48}F_6N_2O_2P_3Re$	$C_{46}H_{48}F_6N_2O_2P_3Re$	$C_{24}H_{33}F_6N_2O_3P_2Re$	$C_{28}H_{33}F_6N_2O_3P_2Re$	$C_{32}H_{33}F_6N_2O_3P_2Re$	$C_{36}H_{33}F_6N_2O_3P_2Re$
fw	833.76	980.48	861	1053.97	759.66	807.70	855.74	903.78
cryst system	Monoclinic	Triclinic	Monoclinic	Monoclinic	Monoclinic	Triclinic	Monoclinic	Triclinic
space group	$P2_1/c$	P-1	$P2_1/c$	C2/c	$P2_1/n$	P-1	$P2_1/n$	P-1
a (Å)	10.462(1)	10.5691(6)	23.173(2)	42.450(4)	8.7506(3)	10.7455(9)	9.327(1)	11.694(1)
b (Å)	15.724(2)	12.4434(8)	15.547(1)	10.1296(9)	10.9321(4)	12.292(1)	19.497(2)	13.536(2)
c (Å)	19.766(3)	17.083(1)	21.324(2)	30.348(3)	29.4316(11)	13.353(1)	17.659(2)	13.657(2)
α (deg)	90	100.042(1)	90	90	90	65.584(1)	90	68.440(3)
β (deg)	98.111(3)	91.437(1)	117.133(1)	130.284(1)	90.9445(12)	70.251(1)	94.463(2)	70.666(4)
γ (deg)	90	106.144(1)	90	90	90	83.092(1)	90	64.490(4)
V (Å^3)	3219.2(7)	2118.6(2)	6836.9(9)	9955(2)	2815.1(2)	1511.1(2)	3201.5(6)	1775.6(4)
Z	4	2	8	8	4	2	4	2
ρ (g/cm^3)	1.720	1.537	1.675	1.406	1.792	1.775	1.775	1.690
T (K)	100	223	100	100	100	100	100	100
μ (mm^{-1})	3.988	3.052	3.758	2.596	4.499	4.197	3.967	3.582
λ souce (Å)	0.71073	0.71073	0.71073	0.71073	0.71073	0.71073	0.71073	0.71073
R(F)[a]	0.0289	0.0326	0.0263	0.0196	0.0307	0.0180	0.0208	0.0812
Rw(F)[2]	0.0459	0.0667	0.0473	0.0426	0.0643	0.0391	0.0421	0.1896
GoF	1.005	1.017	0.944	1.025	1.390	1.036	1.350	1.193

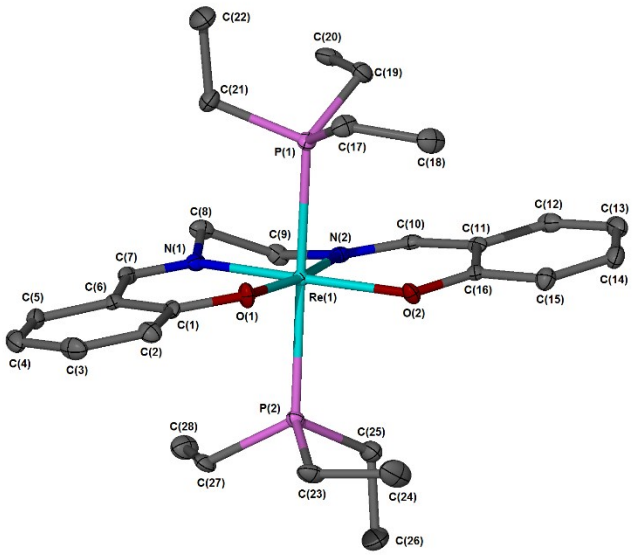

Figure S1. X-ray crystal structure of **2** with 50% probability thermal ellipsoids. Only the cation is shown.

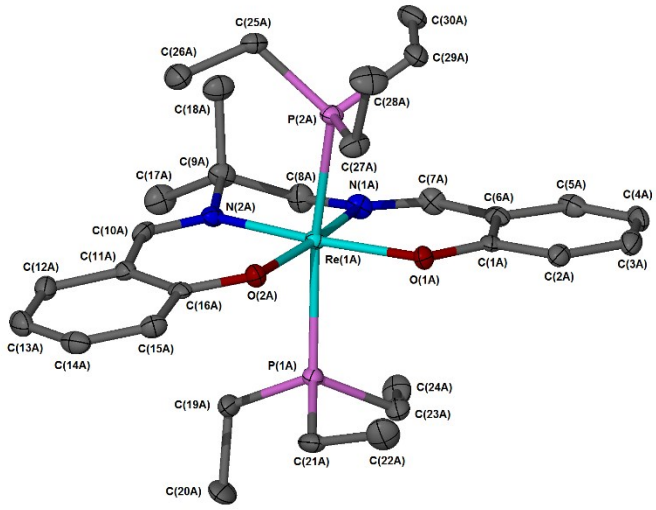

Figure S2. X-ray crystal structure of **5** with 50% probability thermal ellipsoids. Only the cation is shown.

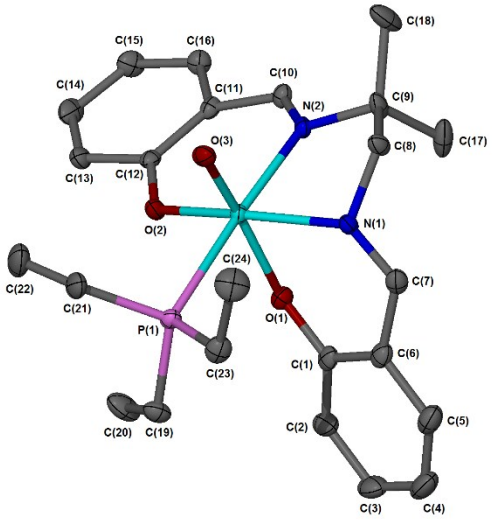

Figure S3. X-ray crystal structure of **8** with 50% probability thermal ellipsoids. Only the cation is shown.

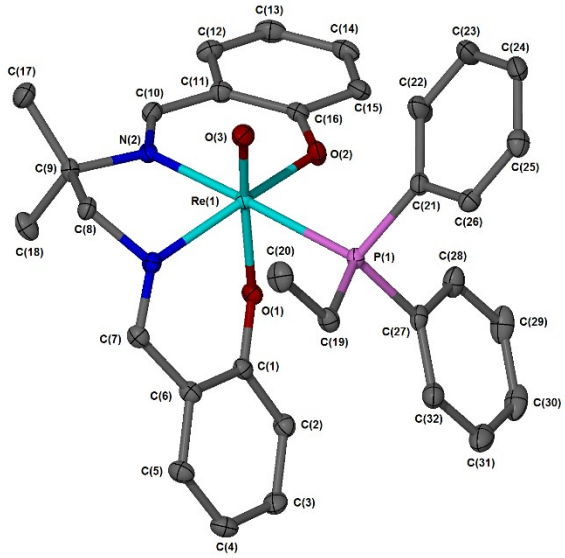

Figure S4. X-ray crystal structure of **9** with 50% probability thermal ellipsoids. Only the cation is shown.

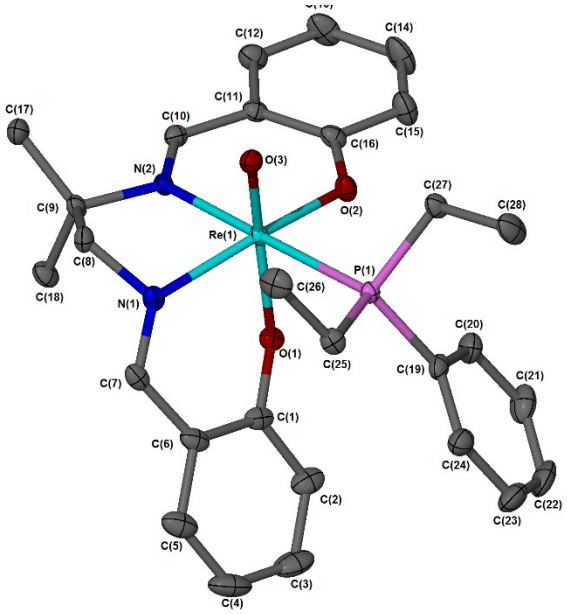

Figure S5. X-ray crystal structure of **10** with 50% probability thermal ellipsoids. Only the cation is shown.

Supplemental Information Section 2. *[1]H-NMR spectra for compounds* ***2-11***

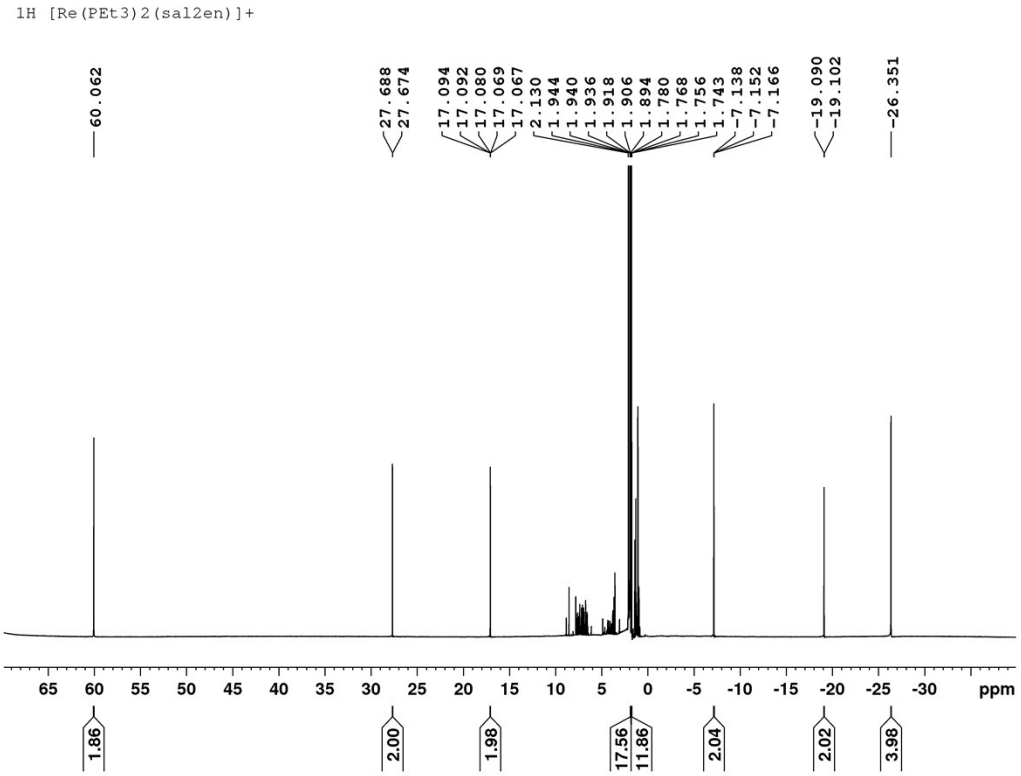

Figure S6. Full view of ^{1}H NMR of **2** *trans*-[Re(PEt_3)$_2$(sal_2en)][PF_6] in CD_3CN (600 MHz, calibrated to residual CHD_2CN at 1.94 ppm).

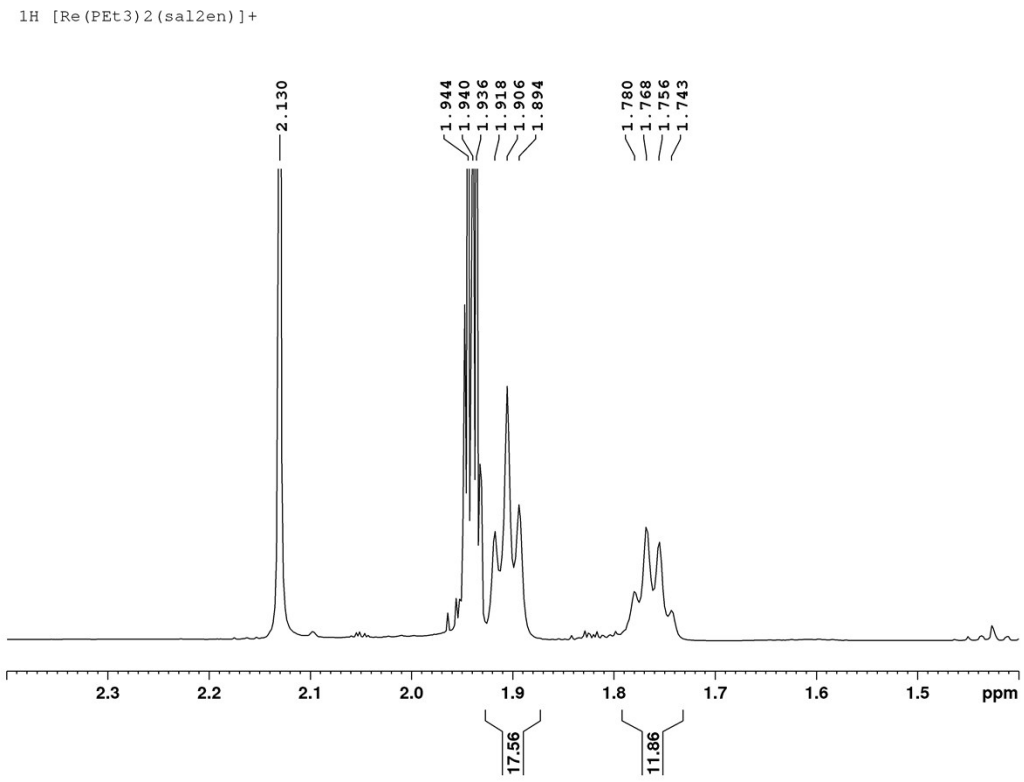

Figure S7. Narrow view of ^{1}H NMR of **2** *trans*-[Re(PEt$_3$)$_2$(sal$_2$en)][PF$_6$] in CD$_3$CN (600 MHz, calibrated to residual CHD$_2$CN at 1.94 ppm).

^{1}H NMR [600 MHz, CD$_3$CN, r.t., δ (ppm)]: 60.06 (s, 2H, -**H**C=N-); 27.68 (d, *J* = 8.3 Hz, 2H, Ar**H**); 17.08 (t, *J* = 7.5 Hz, 2H, Ar**H**); 1.91 (t, *J* = 7.4 Hz, 18H, PCH$_2$C**H$_3$**); 1.76 (q, J = 7.3 Hz, 12H, PC**H$_2$**CH$_3$); -7.15 (t, *J* = 8.3 Hz, 2H, Ar**H**); -19.10 (d, *J* = 7.4 Hz, 2H, Ar**H**); -26.35 (s, 4H, -NC**H$_2$**C**H$_2$**N-).

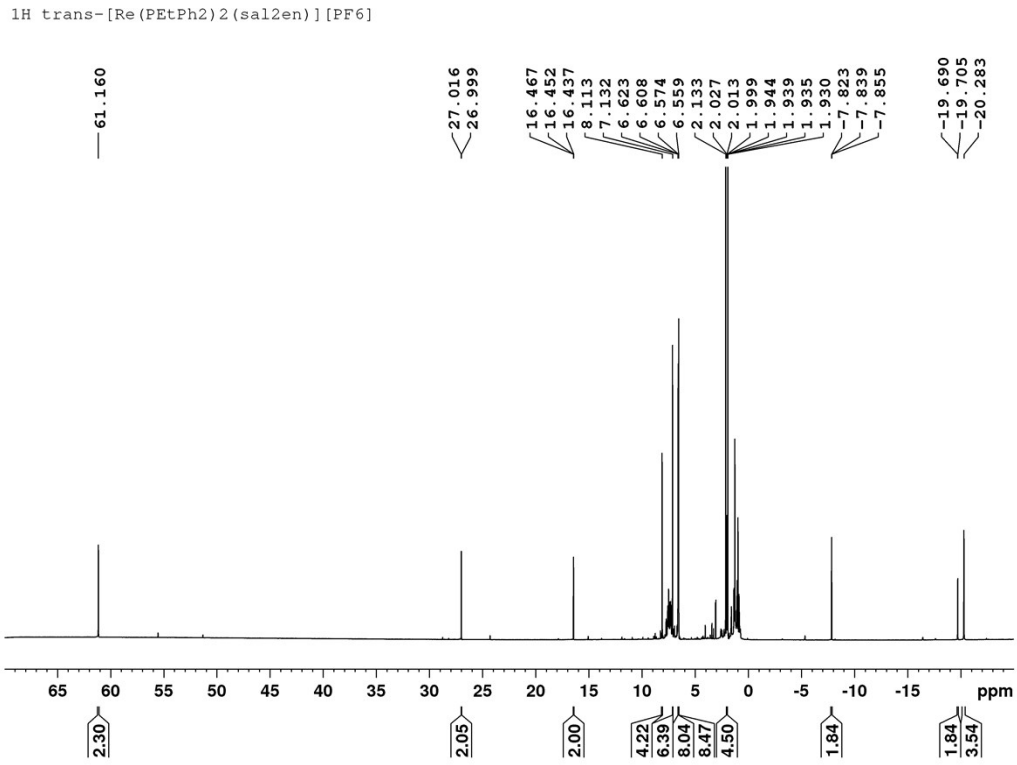

Figure S8. Full view of ^{1}H NMR of **3** *trans*-[Re(PEtPh$_2$)$_2$(sal$_2$en)]Cl in CD_3CN (500 MHz, calibrated to residual CHD_2CN at 1.94 ppm).

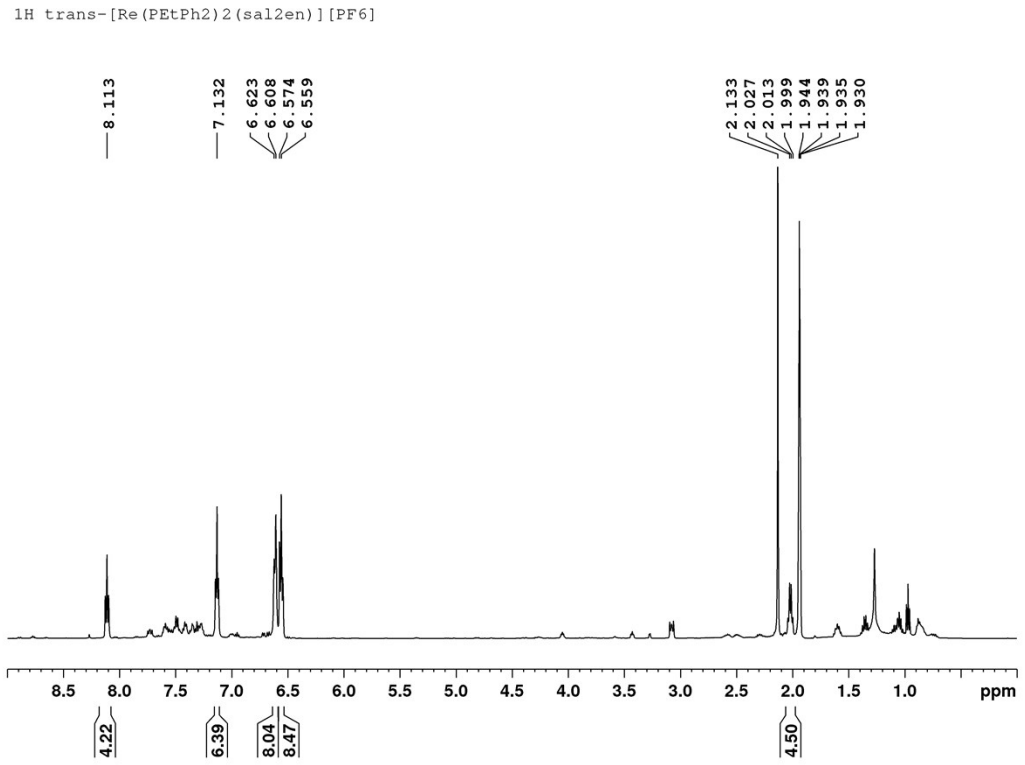

Figure S9. Narrow view of ^{1}H NMR of **3** *trans*-[Re(PEtPh$_2$)$_2$(sal$_2$en)]Cl in CD_3CN (500 MHz, calibrated to residual CHD_2CN at 1.94 ppm).

^{1}H NMR [500 MHz, CD_3CN, r.t., δ (ppm)]: 61.16 (s, 2H, -**H**C=N-); 27.00 (d, *J* = 8.2 Hz, 2H, Ar**H**); 16.45 (t, *J* = 7.3 Hz, 2H, Ar**H**); 8.11 (t, *J* = 7.4 Hz, 4H, P**Ph** para); 7.13 (t, *J* = 6.7 Hz, 6H, PCH$_2$C**H$_3$**); 6.61 (d, *J* = 7.7, 8H, P**Ph** ortho); 6.56 (br s, 8H, P**Ph** meta); 2.10 (q, J = 7.2 Hz, 4H, PC**H$_2$**CH$_3$); -7.84 (t, *J* = 8.0 Hz, 2H, Ar**H**); -19.70 (d, *J* = 7.8 Hz, 2H, Ar**H);** -20.28 (s, 4H, -NC**H$_2$**C**H$_2$**N-).

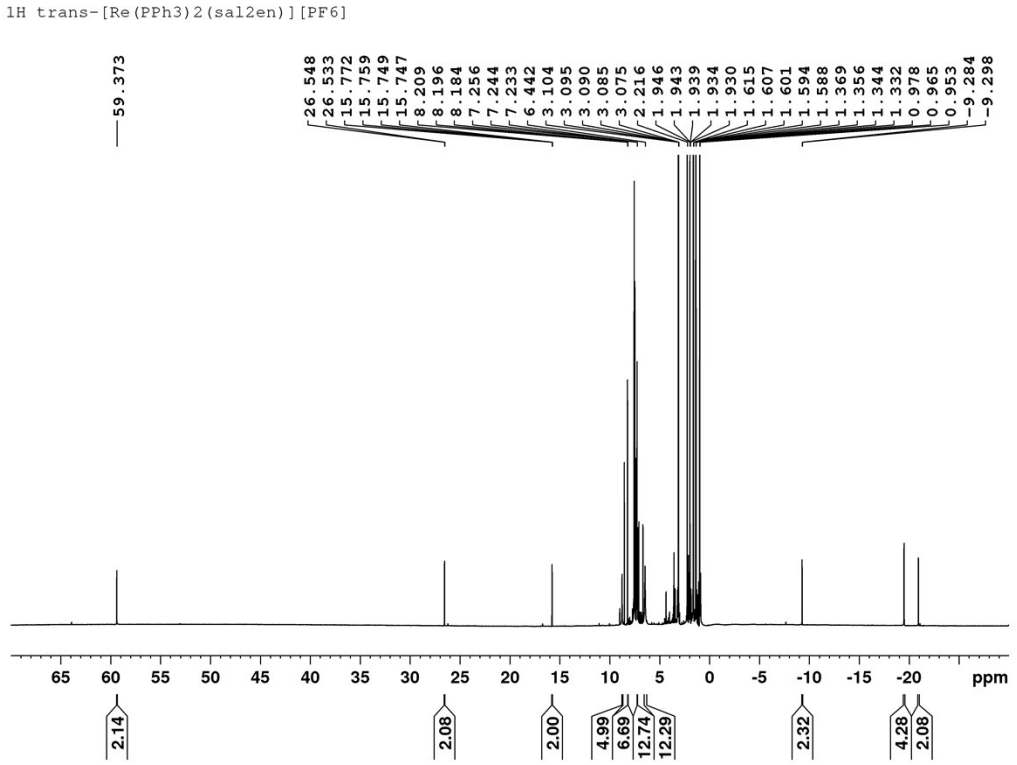

Figure S10. Full view of ^{1}H NMR of **4** *trans*-[Re(PPh$_3$)$_2$(sal$_2$en)][PF$_6$] in CD$_3$CN (600 MHz, calibrated to residual CHD$_2$CN at 1.94 ppm).

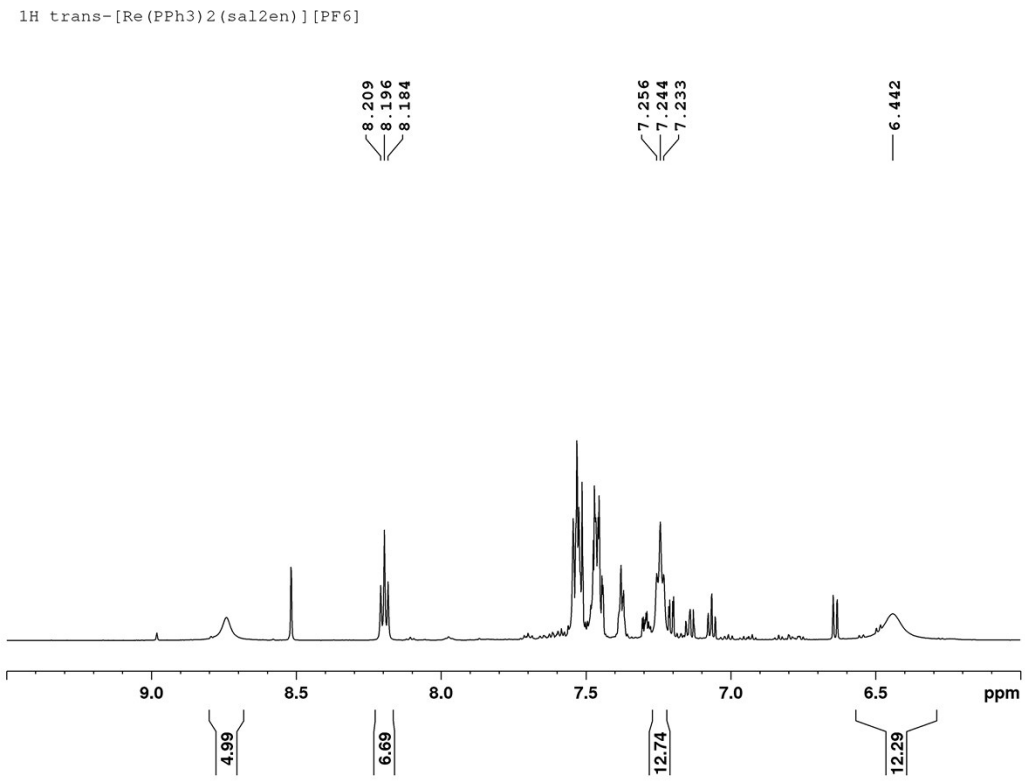

Figure S11. Narrow view of ^{1}H NMR of **4** *trans*-[Re(PPh$_3$)$_2$(sal$_2$en)][PF$_6$] in CD_3CN (600 MHz, calibrated to residual CHD_2CN at 1.94 ppm).

^{1}H NMR [600 MHz, CD_3CN, r.t., δ (ppm)]: 59.37 (s, 2H, -**H**C=N-); 26.54 (d, *J* = 7.8 Hz, 2H, Ar**H**); 15.75 (t, *J* = 7.5 Hz, 2H, Ar**H**); 8.20 (t, *J* = 7.6 Hz, 6H, P**Ph** meta); 7.24 (t, *J* = 7.1 12H, P**Ph** meta); 6.44 (br s, 12H, P**Ph** ortho); -9.30 (t, *J* = 8.1 Hz, 2H, Ar**H**); -19.51 (s, 4H, -NC**H$_2$**C**H$_2$**N-); -20.94 (d, *J* = 7.5 Hz, 2H, Ar**H**).

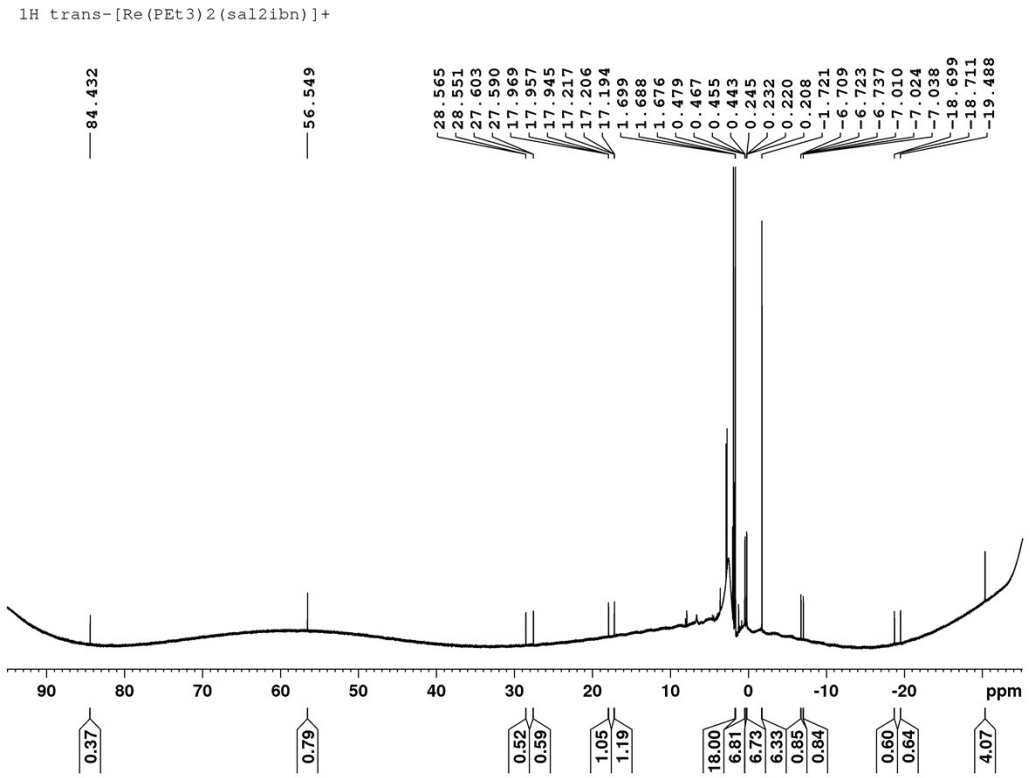

Figure S12. Full view of ^{1}H NMR of **5** *trans*-[Re(PEt$_3$)$_2$(sal$_2$ibn)][PF$_6$] in CD_3CN (600 MHz, calibrated to residual CHD_2CN at 1.94 ppm).

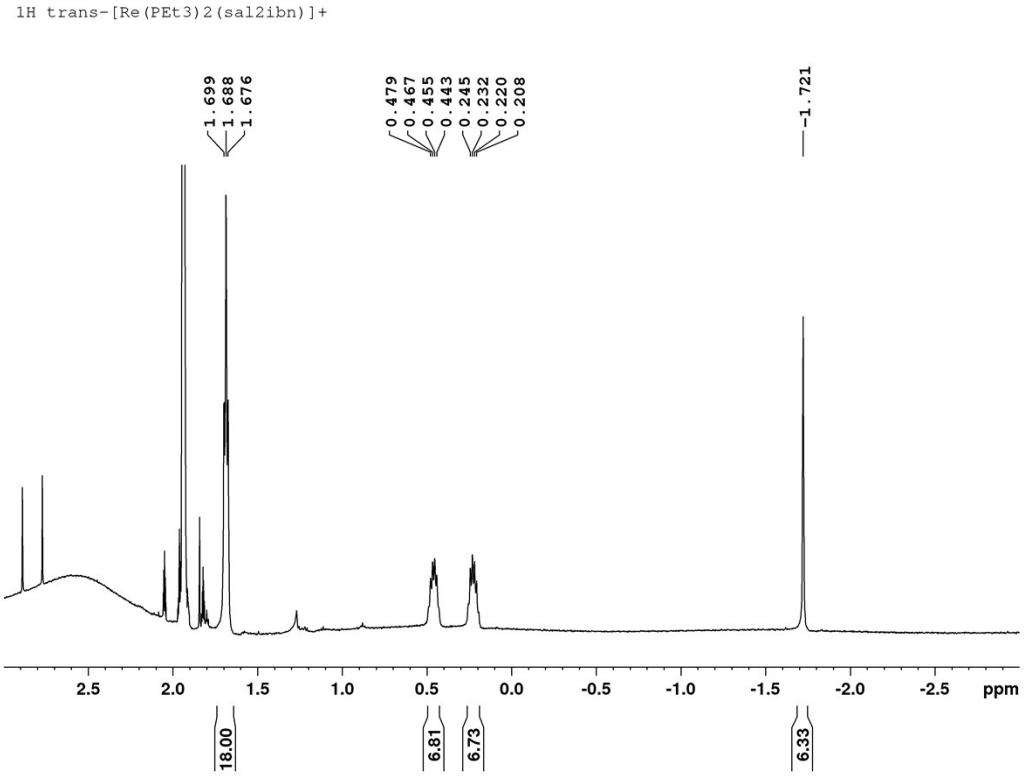

Figure S13. Narrow view of ^{1}H NMR of **5** *trans*-[Re(PEt$_3$)$_2$(sal$_2$ibn)][PF$_6$] in CD_3CN (600 MHz, calibrated to residual CHD_2CN at 1.94 ppm).

^{1}H NMR [600 MHz, CD_3CN, r.t., δ (ppm)]: 84.49 (s, 1H, -**H**C=N-); 56.59 (s, 1H, -**H**C=N-); 28.75 (d, *J* = 8.2 Hz, 1H, Ar**H**); 27.75 (d, *J* = 8.3 Hz, 1H, Ar**H**); 18.03 (t, *J* = 7.1 Hz, 1H, Ar**H**); 17.25 (t, *J* = 7.0 Hz, 1H, Ar**H**); 1.65 (s, 18H, P($CH_2C\mathbf{H_3}$)$_3$); 0.64-0.54 (br m, 6H, P($C\mathbf{H_2}CH_3$)$_3$); 0.34-0.25 (br m, 6H, P($C\mathbf{H_2}CH_3$)$_3$); -1.65 (s, 6H, -C($C\mathbf{H_3}$)$_2CH_2$-); -6.66 (t, *J* = 8.3 Hz, 1H, Ar**H**); -6.95 (t, *J* = 8.3 Hz, 1H, Ar**H**); -18.96 (d, *J* = 7.1 Hz, 1H, Ar**H**); -19.75 (d, *J* = 7.1 Hz, 1H, Ar**H**); -31.06 (s, 2H, -$C(CH_3)_2C\mathbf{H_2}$-).

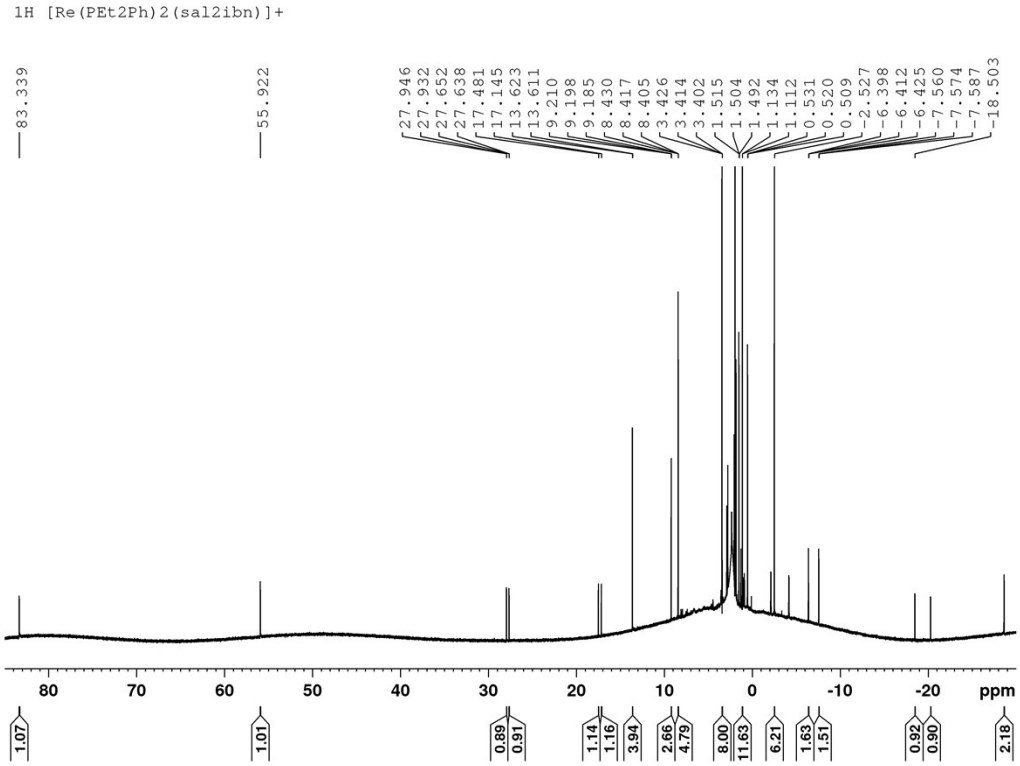

Figure S14. Full view of ^{1}H NMR of **6** *trans*-[Re(PEt_2Ph)$_2$(sal_2ibn)][PF_6] in CD_3CN (600 MHz, calibrated to residual CHD_2CN at 1.94 ppm).

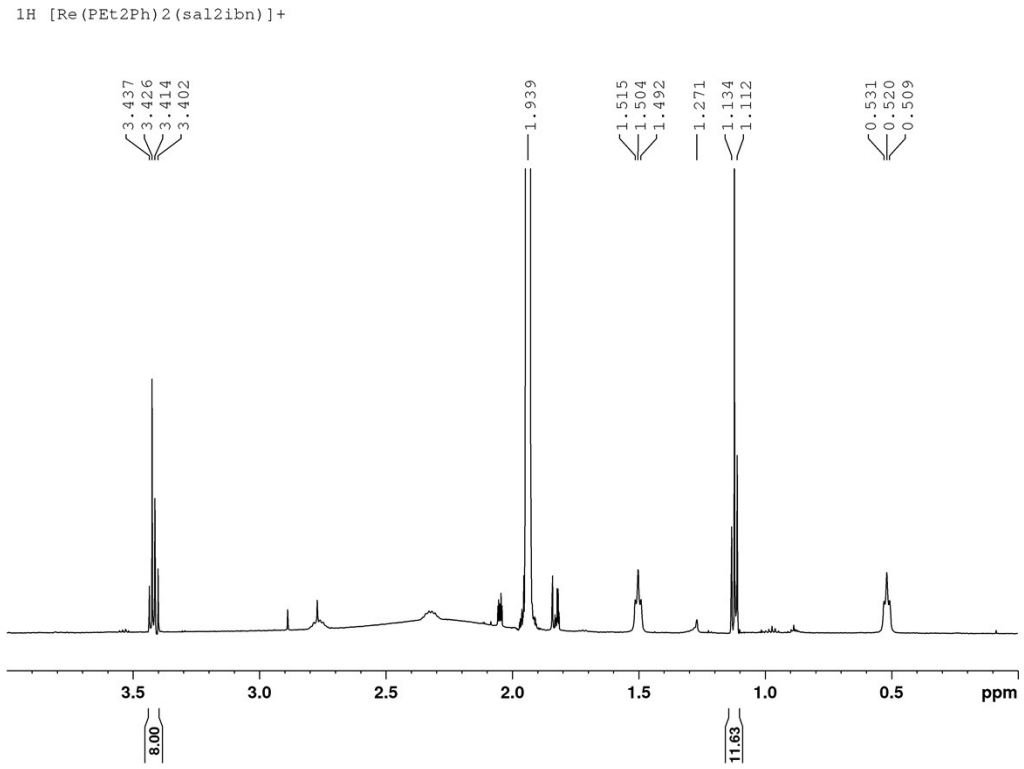

Figure S15. Narrow view of ^{1}H NMR of **6** *trans*-[Re(PEt$_2$Ph)$_2$(sal$_2$ibn)][PF$_6$] in CD_3CN (600 MHz, calibrated to residual CHD_2CN at 1.94 ppm).

^{1}H NMR [600 MHz, CD_3CN, r.t., δ (ppm)]: 83.34 (s, 1H, -C**H**=N-); 55.92 (s, 1H, -C**H**=N-); 27.94 (d, *J* = 8.2 Hz, 1H, Ar**H**); 27.64 (d, *J* = 8.5 Hz, 1H, Ar**H**); 17.48 (t, *J* = 6.6 Hz, 1H, Ar**H**); 17.15 (t, *J* = 7.5 Hz, 1H, Ar**H**); 13.62 (d, *J* = 7.5 Hz, 4H, P**Ph** *ortho*); 9.20 (t, *J* = 7.4 Hz, 2H, P**Ph** *para*); 8.42 (t, *J* = 7.6 Hz, 4H, P**Ph** *meta*); 3.41 (q, *J* = 6.7 Hz, 8H, PC**H$_2$**CH$_3$); 1.12 (t, *J* = 6.6 Hz, 12H, PCH$_2$C**H$_3$**); -2.53 (s, 6H, -C(C**H$_3$**)$_2$CH$_2$-); -6.41 (t, *J* = 8.2 Hz, 1H, Ar**H**); -7.57 (t, *J* = 8.2 Hz, 1H, Ar**H**); -18.51 (d, *J* = 7.2 Hz, 1H, Ar**H**); -20.29 (d, *J* = 7.1 Hz, 1H, Ar**H**); -28.65 (s, 2H, -C(CH$_3$)$_2$C**H$_2$**-).

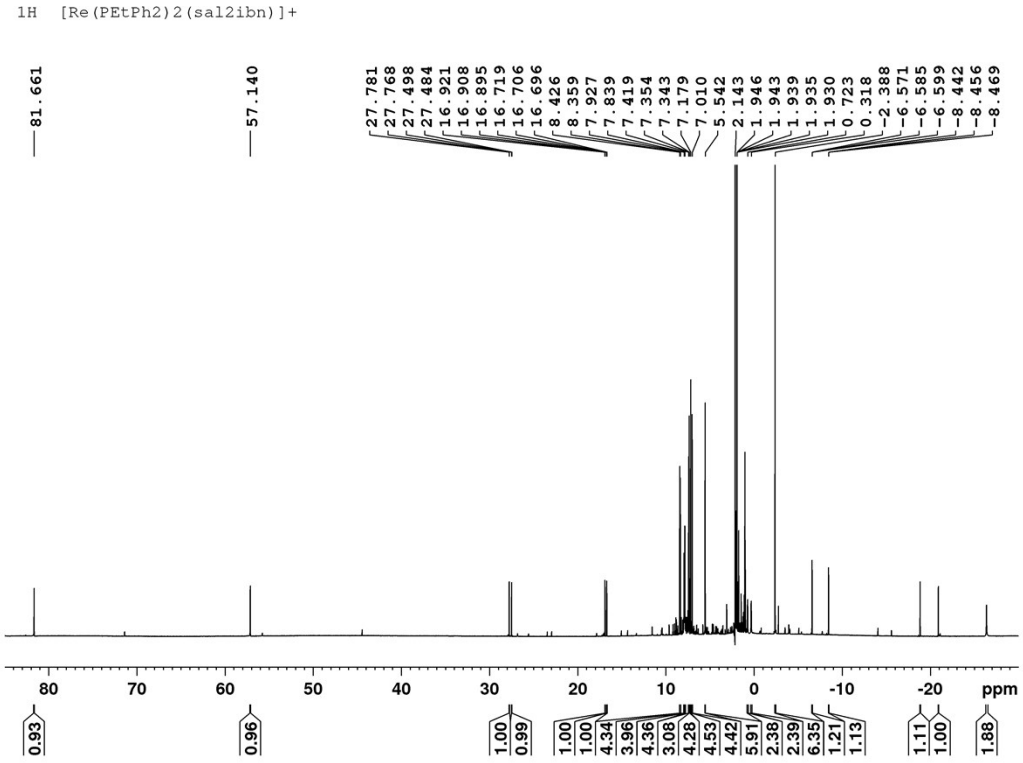

Figure S16. Full view of ^{1}H NMR of **7** *trans*-[Re(PEtPh$_2$)$_2$(sal$_2$ibn)][PF$_6$] in CD$_3$CN (600 MHz, calibrated to residual CHD$_2$CN at 1.94 ppm).

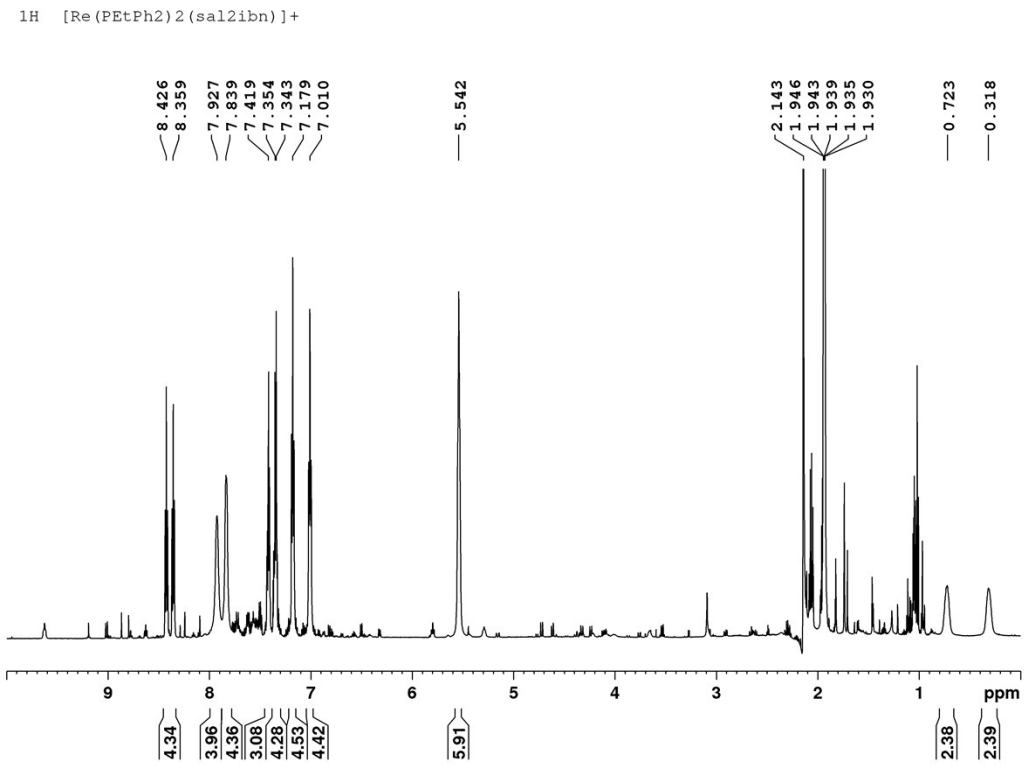

Figure S17. Narrow view of ^{1}H NMR of **7** *trans*-[Re(PEtPh$_2$)$_2$(sal$_2$ibn)][PF$_6$] in CD$_3$CN (600 MHz, calibrated to residual CHD$_2$CN at 1.94 ppm).

^{1}H NMR [600 MHz, CD$_3$CN, r.t., δ (ppm)]: 81.68 (s, 1H, -C**H**=N-); 57.17 (s, 1H, -C**H**=N-); 27.78 (d, *J* = 8.2 Hz, 1H, Ar**H**); 27.50 (d, *J* = 8.2 Hz, 1H, Ar**H**); 16.91 (t, *J* = 7.6 Hz, 1H, Ar**H**); 16.71 (t, *J* = 7.4 Hz, 1H, Ar**H**); 8.43 (t, *J* = 7.6 Hz, 2H, P**Ph** para); 8.36 (t, *J* = 7.3 Hz, 2H, P**Ph** para); 7.93 (br s, 4H, P**Ph** ortho); 7.84 (br s, 4H, P**Ph** ortho); 7.18 (t, *J* = 7.6 Hz, 4H, P**Ph** meta); 7.01 (t, *J* = 7.4 Hz, 4H, P**Ph** meta); 5.54 (m, 6H, PCH$_2$C**H$_3$**); 0.72 (br s, 2H, PC**H$_2$**CH$_3$); 0.31 (br s, 2H, PC**H$_2$**CH$_3$); -2.39 (s, 6H, -C(C**H$_3$**)$_2$CH$_2$-); -6.59 (t, *J* = 8.2 Hz, 1H, Ar**H**); -8.46 (t, *J* = 8.2 Hz, 1H, Ar**H**); -18.85 (d, *J* = 7.3 Hz, 1H, Ar**H**); -20.92 (d, *J* = 7.3 Hz, 1H, Ar**H**); -26.39 (s, 2H, -C(CH$_3$)$_2$C**H$_2$**-).

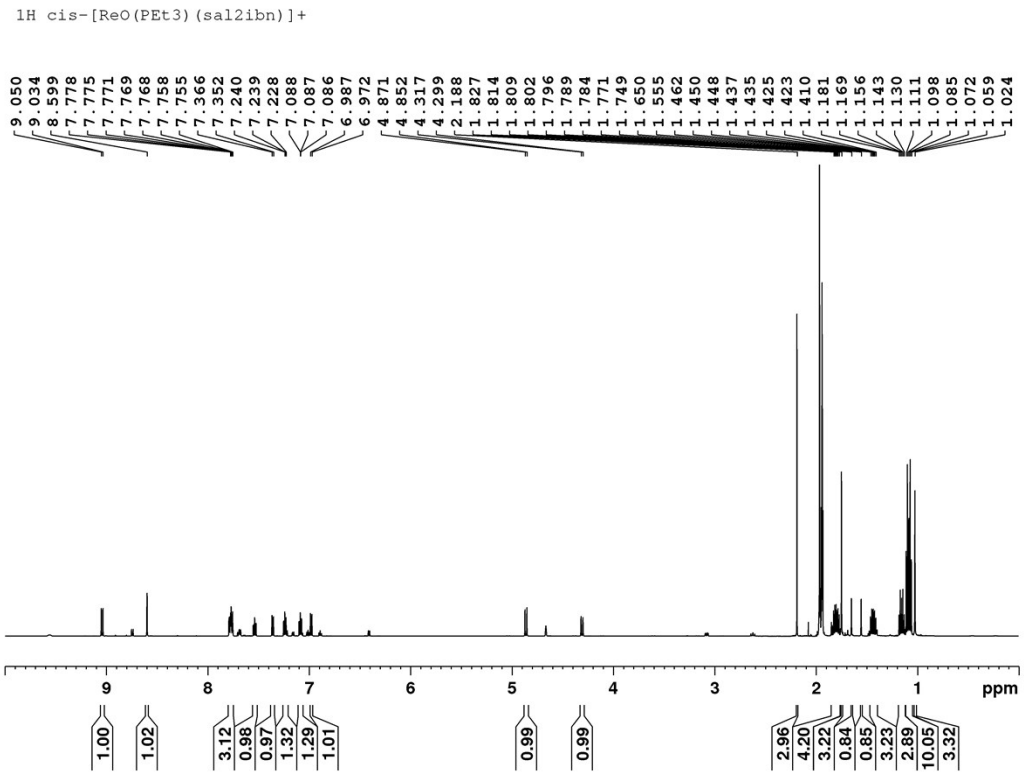

Figure S18. ^{1}H NMR of **8** *cis*-[ReO(PEt$_3$)(sal$_2$ibn)][PF$_6$] in CD$_3$CN (500 MHz, calibrated to residual CHD$_2$CN at 1.94 ppm).

^{1}H NMR [600 MHz, CD$_3$CN, r.t., δ (ppm)]: 9.04 (d, *J* = 9.7 Hz, 1H, -**H**C=N-); 8.60 (s, 1H, -**H**C=N-); 7.75-7.79 (m, Ar**H**, 3H); 7.52-7.55 (m, Ar**H,** 1H); 7.35 (m, 1H, Ar**H**); 7.24 (m, 1H, Ar**H**); 7.09 (m, Ar**H**, 1H); 6.98 (d, *J* = 8.5 Hz, 1H, Ar**H**); 4.86 (d, *J* = 11.1 Hz, 1H, -NC**H**$_2$-C(CH$_3$)); 4.30 (d, *J* = 11.0 Hz, 1H, -NC**H**$_2$-C(CH$_3$)); 1.77-1.85 (m, 3H, PC**H**$_2$CH$_3$); 1.75 (s, 3H, -C**H$_3$**); 1.41-1.46 (m, 1H, PC**H**$_2$CH$_3$); 1.06-1.11 (m, 9H, PCH$_2$C**H**$_3$) 1.02 (s, 3H, -C**H$_3$**).

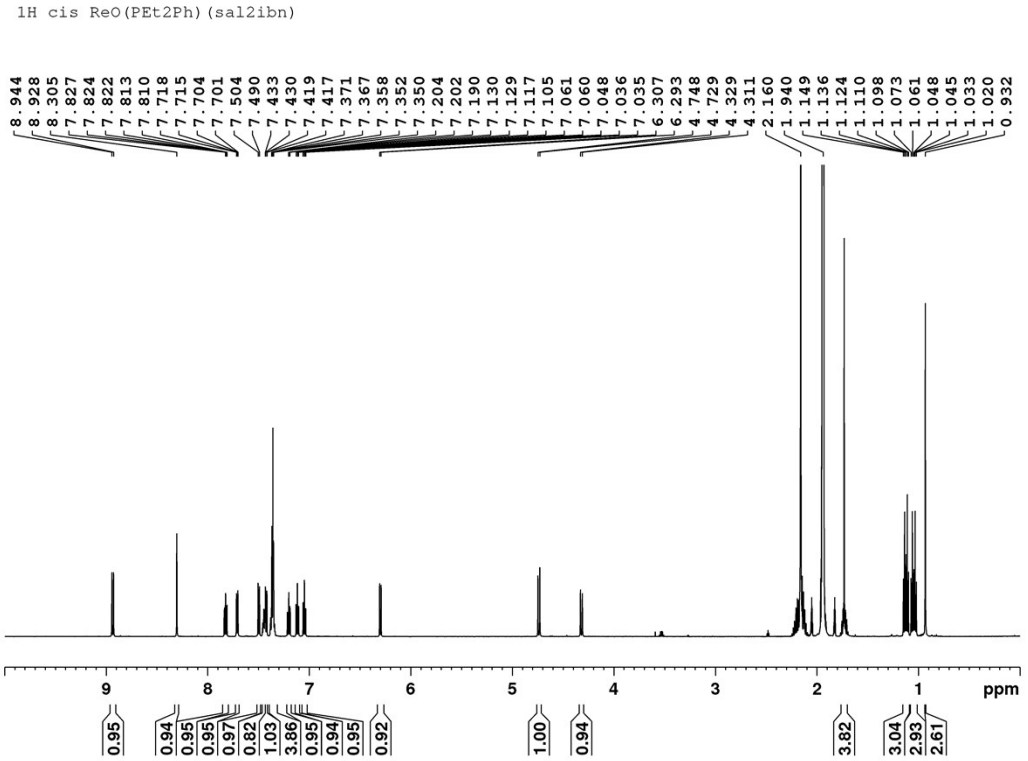

Figure S19. ^{1}H NMR of **9** *cis*-[ReO(PEt_2Ph)(sal_2ibn)][PF_6] in CD_3CN (500 MHz, calibrated to residual CHD_2CN at 1.94 ppm).

^{1}H NMR [600 MHz, CD_3CN, r.t., δ (ppm)]: 8.94 (d, 1H, -**H**C=N-); 8.05 (s, 1H, -**H**C=N-); 7.82 (m, *J* = 1.4, 7.7 Hz, 1H, Ar**H**); 7.72, 7.70 (dd, *J* = 1.8, 7.9 Hz, 1H, Ar**H**); 7.50, 7.49 (d, J =8.4 Hz, 1H, Ar**H**); 7.47-7.45 (m, 1H, P**Ph** *para*); 7.37-7.35 (m, 4H, P**Ph**); 7.43, 7.42 (dd, *J* = 1.7, 8.0 Hz, 1H, Ar**H**); 7.20 (m, *J* = 1.7, 6.3 Hz, 1H, Ar**H**); 7.12 (m, *J* = 1.1, 7.5 Hz, 1H, Ar**H**); 7.05 (m, *J* = 1.0, 7.5 Hz, 1H, Ar**H**); 6.31, 6.29 (d, *J* = 8.5 Hz, 1H, Ar**H**); 4.75, 4.73 (d, *J* = 11 Hz, 1H, -NC**H**$_2$-C(CH_3)); 4.33, 4.31 (d, *J* = 11 Hz, 1H, -NC**H**$_2$-C(CH_3)-); 2.20-2.08 (m, 4H, PC**H**$_2$$CH_3$); 1.76 (s, 3H, -C**H**$_3$); 1.15-1.02 (d of d of t, *J* = 7.5 Hz, 6H, PCH_2C**H**$_3$); 1.01 (s, 3H, -C**H**$_3$).

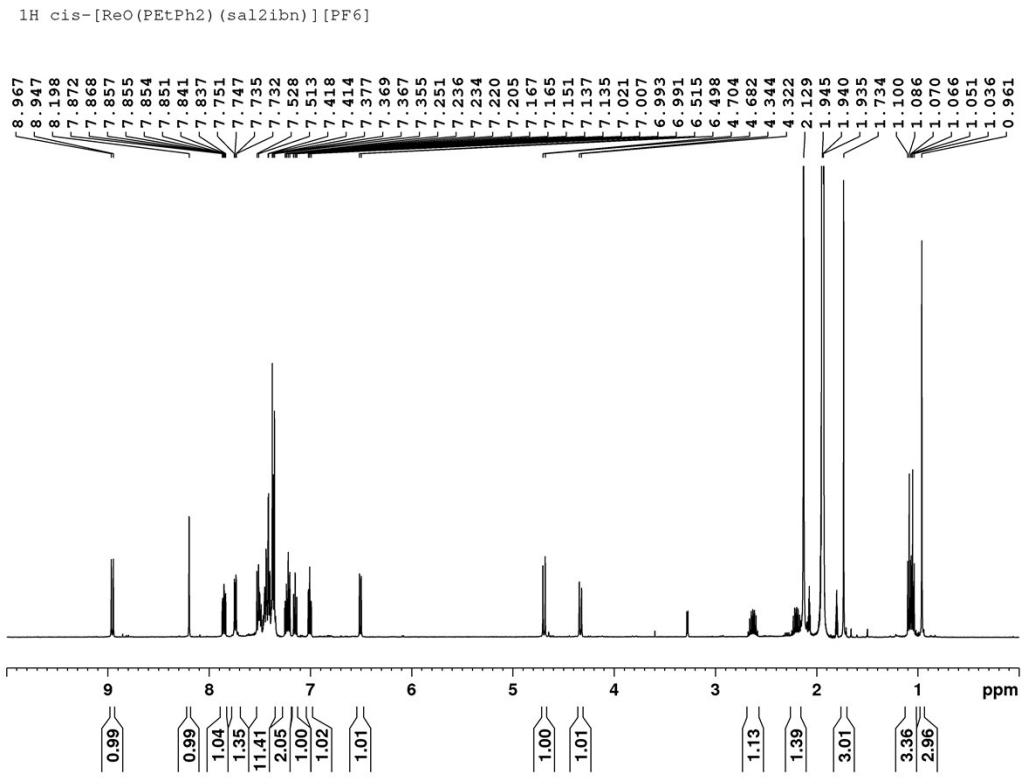

Figure S20. ^{1}H NMR of **10** *cis*-[ReO(PEtPh$_2$)(sal$_2$ibn)][PF$_6$] in CD$_3$CN (500 MHz, calibrated to residual CHD$_2$CN at 1.94 ppm).

^{1}H NMR [500 MHz, CD$_3$CN, r.t., δ (ppm)]: 8.95 (d, *J* = 10 Hz, 1H, -**H**C=N-); 8.20 (s, 1H, -**H**C=N-); 7.87-6.99 (m, Ar**H,** 8H); 7.53-7.36 (m, P**Ph**, 10H); 4.69 (d, *J* = 11 Hz, 1H, -NC**H**$_2$-C(CH$_3$)); 4.33 (d, *J* = 11 Hz, 1H, -NC**H**$_2$-C(CH$_3$)); 2.68-2.58 (m, 1H, PC**H**$_2$CH$_3$); 2.25-2.15 (m, 1H, PC**H**$_2$CH$_3$); 1.73 (s, 3H, -C**H$_3$**); 1.15-1.02 (d of t, *J* = 7.5 Hz, 3H, PCH$_2$C**H**$_3$); 0.96 (s, 3H, -C**H$_3$**).

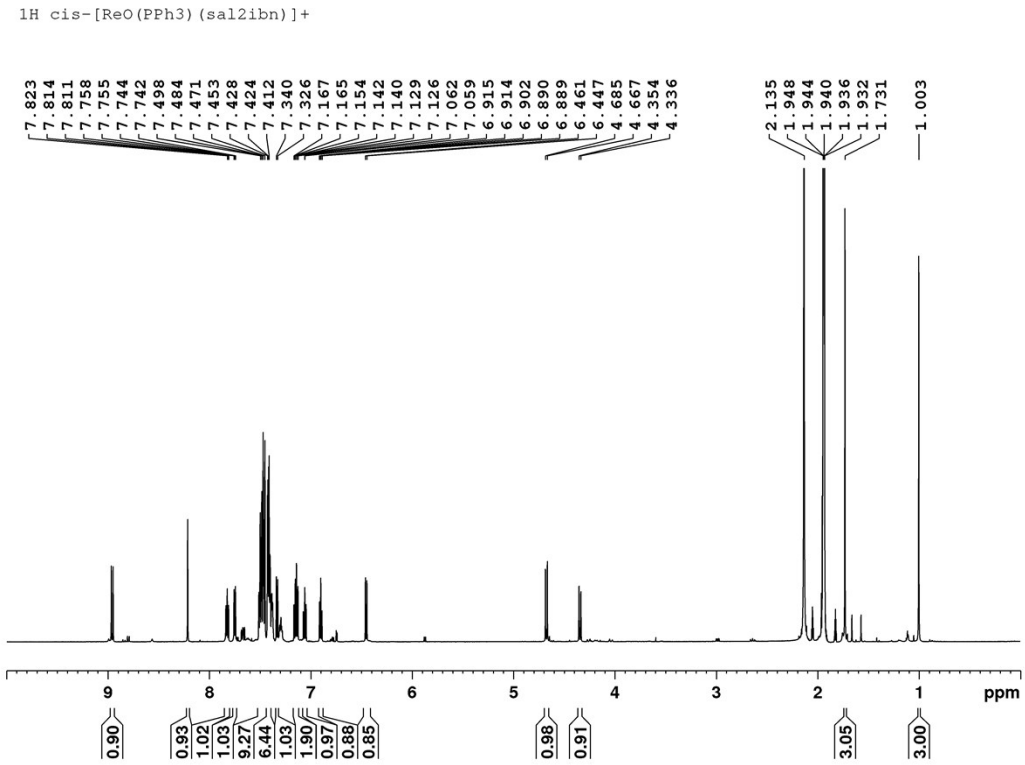

Figure S21. ^{1}H NMR of **11** *cis*-[ReO(PPh_3)(sal_2ibn)][PF_6] in CD_3CN (600 MHz, calibrated to residual CHD_2CN at 1.94 ppm).

^{1}H NMR [600 MHz, CD_3CN, r.t., δ (ppm)]: 8.96 (d, J = 10 Hz, 1H); 8.22 (-**H**C=N-); 7.84-7.74, 7.34-6.44 (m, Ar**H**); 7.52-7.39 (m, P**Ph**, 15H); 4.67 (d, J = 11 Hz, 1H, -NC**H**$_2$-C(CH_3)); 4.34 (d, J = 11 Hz, 1H, -NC**H**$_2$-C(CH_3)); 1.73 (s, 3H, -C**H$_3$**); 1.00 (s, 3H, -C**H$_3$**).

Supplemental Information Section 3. *Cyclic voltammograms for compounds* ***2-7***

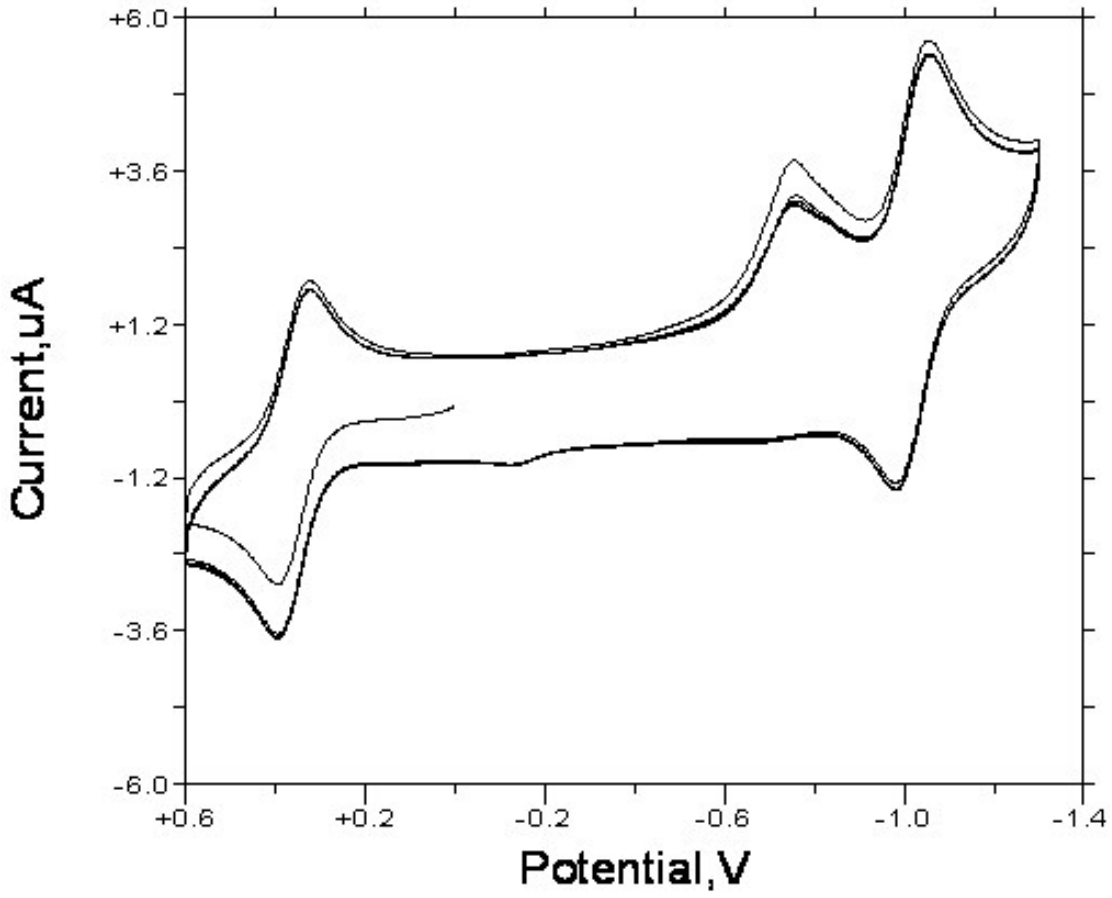

Figure S22. Repetitive cyclic voltammogram (CV) for *trans*-[$Re(PEt_3)_2(sal_2en)$][PF_6] **2** in the region -1.3 to +0.6 V.

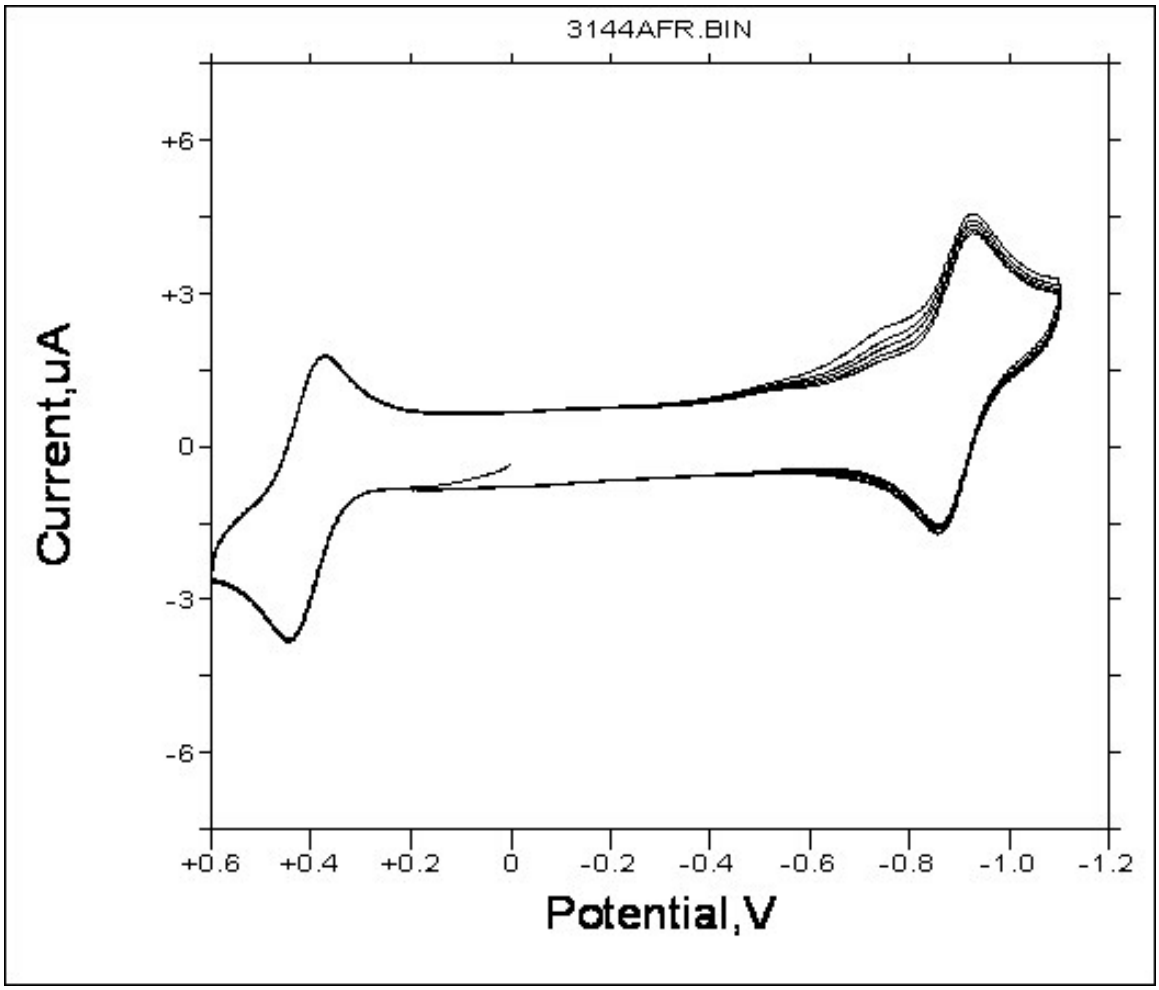

Figure S23. Repetitive CV for *trans*-[$Re(PEtPh_2)_2(sal_2en)][PF_6$] **3** in the region -1.2 to +0.6 V.

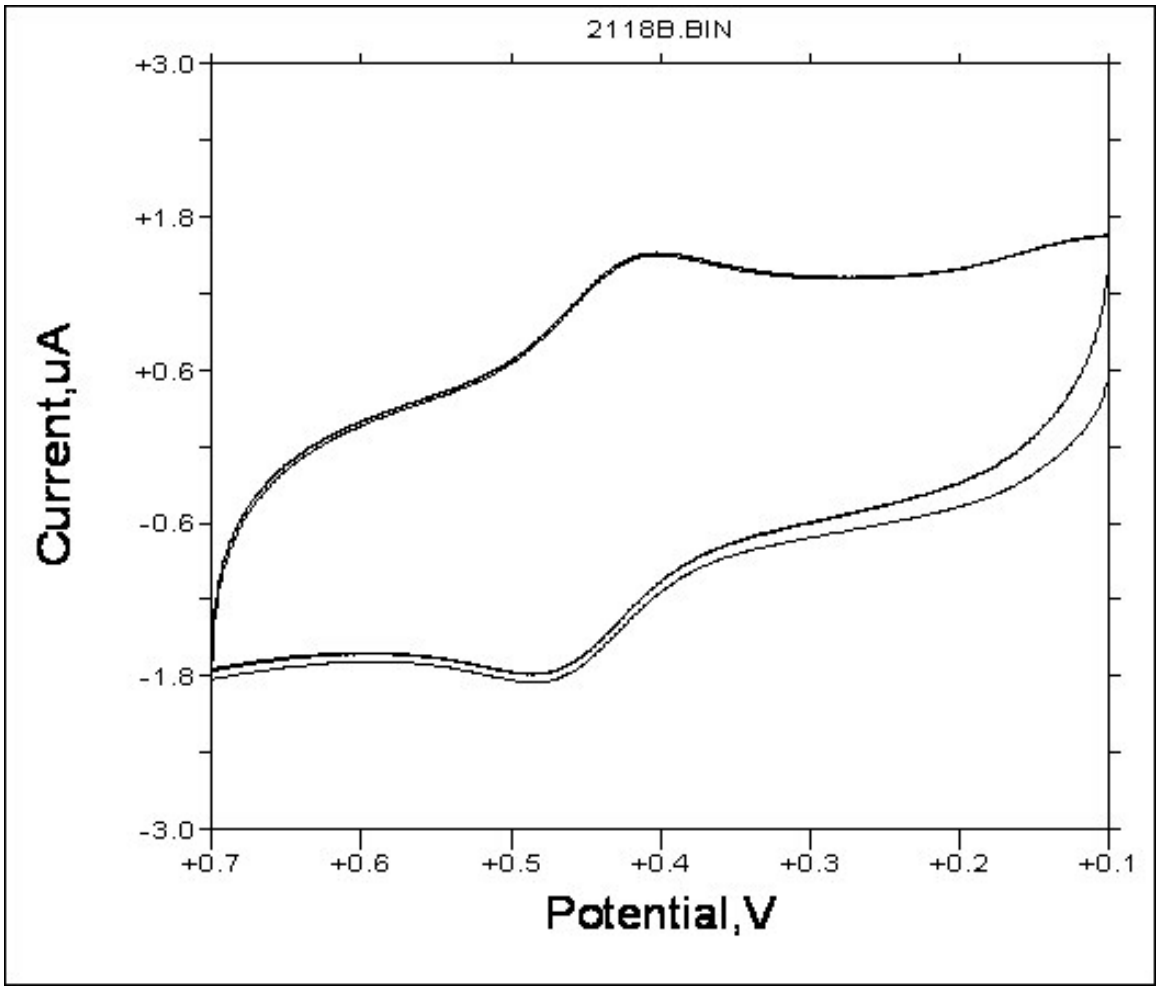

Figure S24. Repetitive CV for *trans*-[$Re(PPh_3)_2(sal_2en)][PF_6$] **4** in the region +0.1 to +0.7 V.

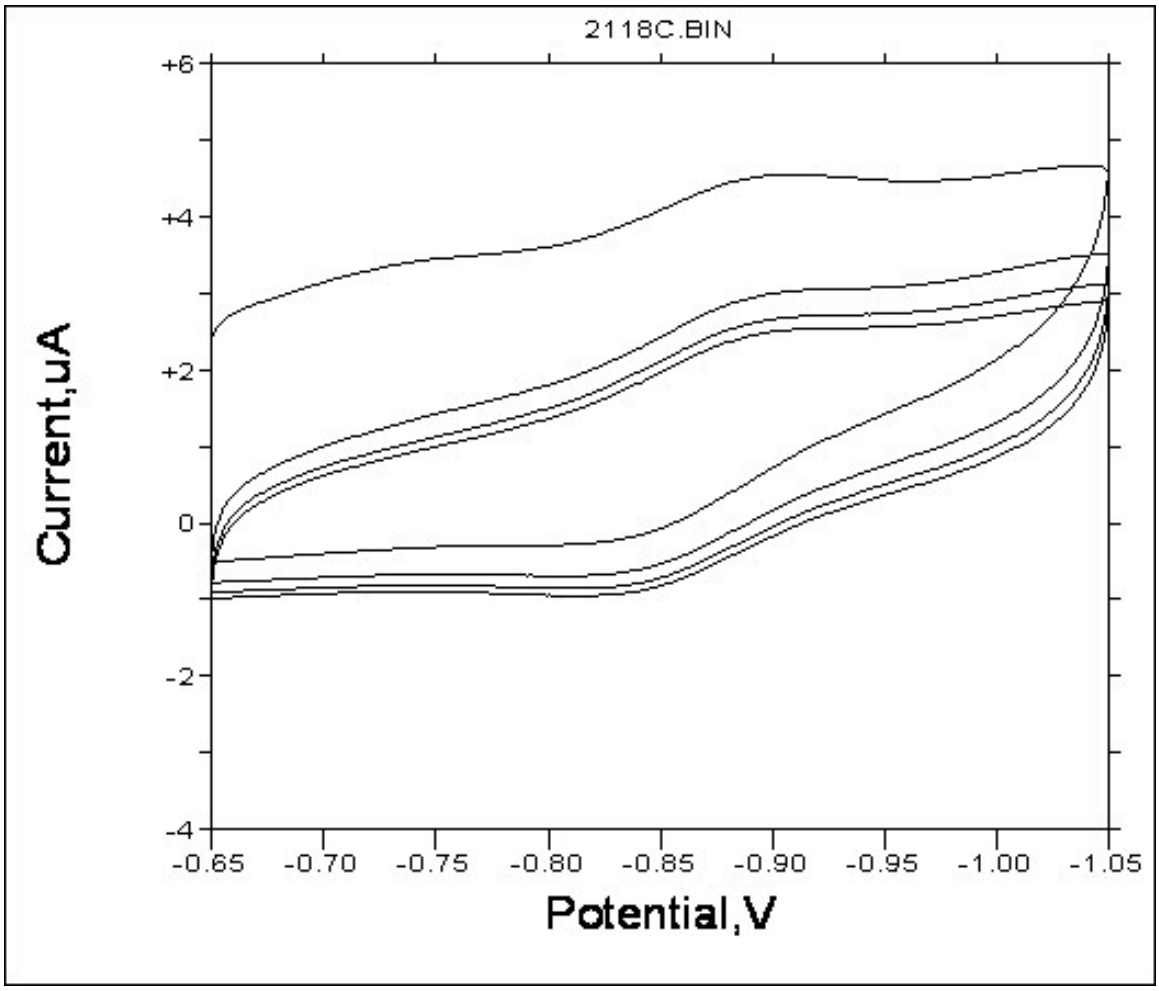

Figure S25. Repetitive CV for *trans*-[$Re(PPh_3)_2(sal_2en)][PF_6$] **4** -1.05 to -0.65 V.

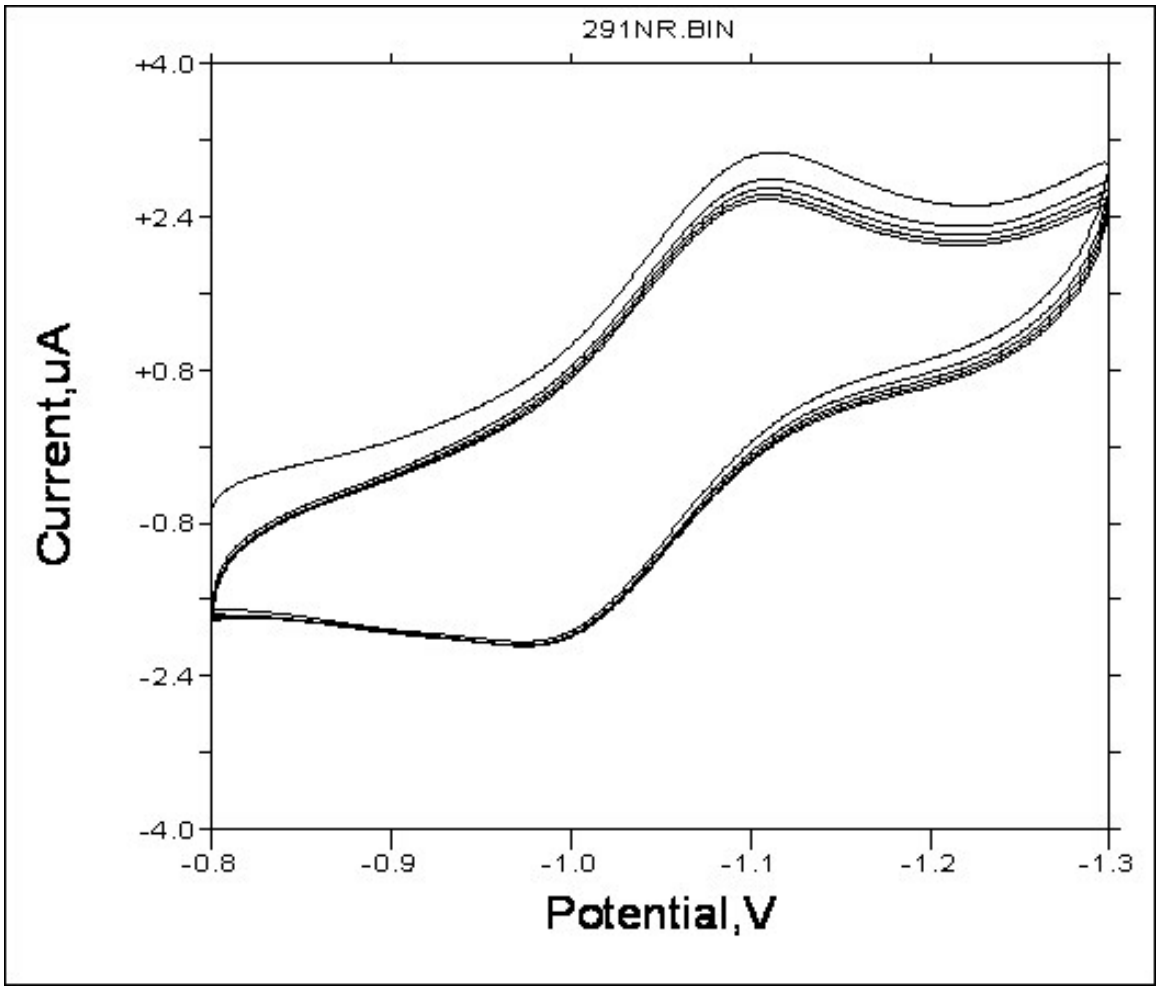

Figure S26. Repetitive CV for *trans*-[$Re(PEt_3)_2(sal_2ibn)][PF_6$] **5** in the region -1.3 to -0.8 V.

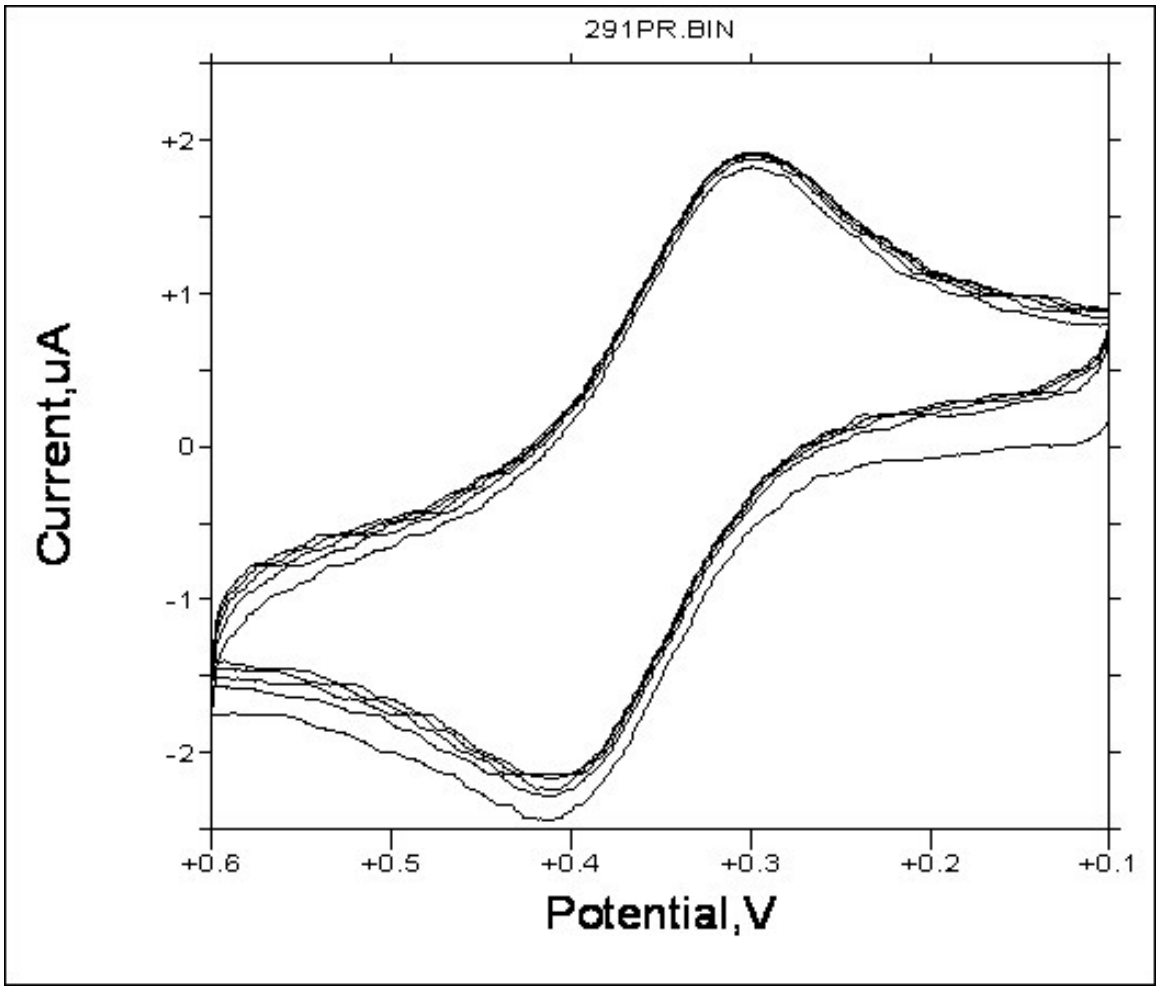

Figure S27. Repetitive CV for *trans*-[$Re(PEt_3)_2(sal_2ibn)][PF_6$] **5** in the region +0.1 to +0.6 V.

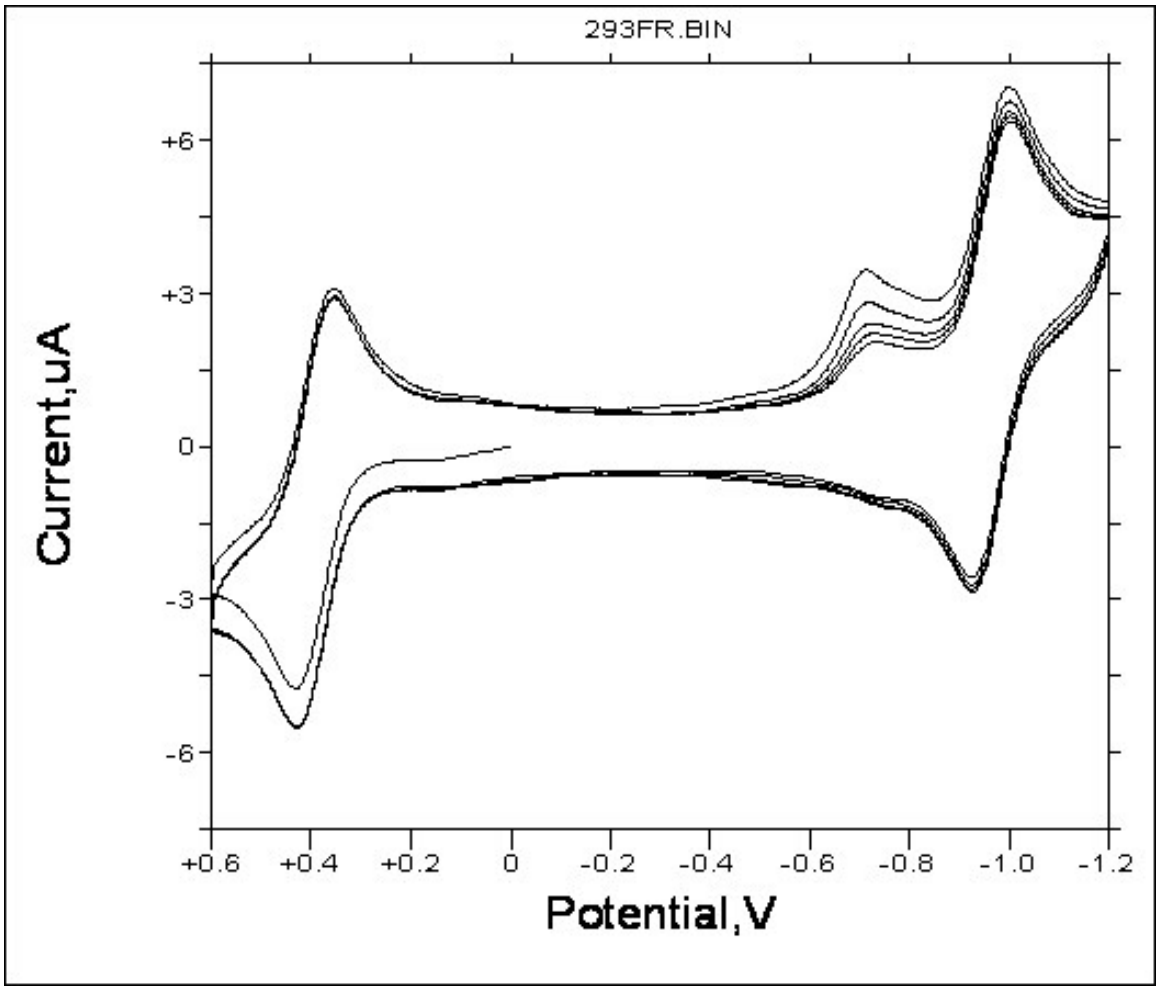

Figure S28. Repetitive CV for *trans*-[$Re(PEtPh_2)_2(sal_2ibn)][PF_6]$ **6** in the region -1.2 to +0.6 V.